chemistry

MDPI

Article

Rare Nuclearities and Unprecedented Structural Motifs in Manganese Cluster Chemistry from the Combined Use of Di-2-Pyridyl Ketone with Selected Diols †

Katerina Skordi [1], Dimitris I. Alexandropoulos [1], Adeline D. Fournet [2,‡], Nikos Panagiotou [1], Eleni E. Moushi [3], Constantina Papatriantafyllopoulou [1,§], George Christou [2] and Anastasios J. Tasiopoulos [1,*]

[1] Department of Chemistry, University of Cyprus, 1678 Nicosia, Cyprus; skordi.katerina@ucy.ac.cy (K.S.); alexandropoulos.dimitrios@ucy.ac.cy (D.I.A.); panagiotou.nikos@ucy.ac.cy (N.P.); constantina.papatriantafyllopo@universityofgalway.ie (C.P.)
[2] Department of Chemistry, University of Florida, Gainesville, FL 32611, USA; adeline.fournet@gmail.com (A.D.F.); christou@chem.ufl.edu (G.C.)
[3] Department of Life Sciences, School of Science, European University Cyprus, 1516 Nicosia, Cyprus; e.moushi@euc.ac.cy
* Correspondence: atasio@ucy.ac.cy
† Dedicated to Professor Spyros P. Perlepes, an excellent scientist, great teacher, valuable collaborator, and dear friend, on the occasion of his 70th birthday.
‡ Current address: Intel Corporation, Hillsboro, OR 97124, USA.
§ Current address: School of Biological and Chemical Sciences, College of Science and Engineering, University of Galway, University Road, H91 TK33 Galway, Ireland.

check for updates

Citation: Skordi, K.; Alexandropoulos, D.I.; Fournet, A.D.; Panagiotou, N.; Moushi, E.E.; Papatriantafyllopoulou, C.; Christou, G.; Tasiopoulos, A.J. Rare Nuclearities and Unprecedented Structural Motifs in Manganese Cluster Chemistry from the Combined Use of Di-2-Pyridyl Ketone with Selected Diols. *Chemistry* **2023**, *5*, 1681–1695. https://doi.org/10.3390/chemistry5030115

Academic Editors: Catherine Housecroft and Miguel Julve

Received: 3 July 2023
Revised: 25 July 2023
Accepted: 27 July 2023
Published: 1 August 2023

Abstract: The combined use of di-2-pyridyl ketone ($(py)_2CO$) with various diols in Mn cluster chemistry has afforded five new compounds, namely, $[Mn_{11}O_2(OH)_2\{(py)_2CO_2\}_5(pd)(MeCO_2)_3(N_3)_3(NO_3)_2(DMF)_4](NO_3)\cdot 2DMF\cdot H_2O$ (**1**·2DMF·H_2O), $[Mn_{11}O_2(OH)_2\{(py)_2CO_2\}_5(mpd)(MeCO_2)_3(N_3)_3(NO_3)_2(DMF)_4](NO_3)$ (**2**), $[Mn_{12}O_4(OH)_2\{(py)_2CO_2\}_4(mpd)_2(Me_3CCO_2)_4(NO_3)_4(H_2O)_6](NO_3)_2\cdot 2MeCN$ (**3**·2MeCN), $[Mn_4(OMe)_2\{(py)_2C(OMe)O\}_2(2\text{-hp})_2(NO_3)_2(DMF)_2]$ (**4**), and $[Mn_7\{(py)_2CO_2\}_4(2\text{-hp})_4(NO_3)_2(DMF)_2](ClO_4)\cdot DMF$ (**5**·DMF) ($(py)_2CO_2^{2-}$ and $(py)_2C(OMe)O^-$ = gem-diol and hemiketal derivatives of di-2-pyridyl ketone, pdH_2 = 1,3-propanediol, $mpdH_2$ = 2-metly-1,3-propanediol, 2-hpH_2 = 2-(hydroxymethyl)phenol). Complexes **1** and **2** are isostructural, possessing an asymmetric $[Mn^{III}_5Mn^{II}_6(\mu_4\text{-O})(\mu_3\text{-O})(\mu_3\text{-OH})(\mu\text{-OH})(\mu_3\text{-OR})_2(\mu\text{-OR})_{10}(\mu\text{-N}_3)]^{8+}$ core. Compound **3** is based on a multilayer $[Mn^{III}_8Mn^{II}_4(\mu_4\text{-O})_2(\mu_3\text{-O})_2(\mu_3\text{-OH})_2(\mu\text{-OR})_{12}]^{10+}$ core, while complex **4** comprises a defective dicubane core. The crystal structure of **5** reveals that it is based on an unusual non-planar $[Mn^{III}_5Mn^{II}_2(\mu\text{-OR})_{12}]^{7+}$ core with a serpentine-like topology. Direct current (dc) magnetic susceptibility studies revealed the presence of dominant antiferromagnetic exchange interactions in complex **3**, while ferromagnetic coupling between the Mn ions was detected in the case of compound **5**. Fitting of the magnetic data for complex **4** revealed weak antiferromagnetic interactions along the peripheral $Mn^{II}\cdots Mn^{III}$ ions (J_{wb} = −0.33 (1) cm^{-1}) and ferromagnetic interactions between the central $Mn^{III}\cdots Mn^{III}$ ions (J_{bb} = 6.28 (1) cm^{-1}).

Keywords: manganese; di-2-pyridyl ketone; metal complexes; cluster chemistry; molecular magnetism

1. Introduction

Polynuclear coordination complexes of paramagnetic 3d metal ions have become the focus of intense investigation over the last few decades since they often possess interesting physical properties and fascinating structural features [1–5]. Among other 3d metals, manganese-containing compounds have been of great interest due to the ability of Mn ions to adopt a variety of oxidation states (i.e., II, III, and IV) and form high nuclearity metal-oxo clusters that can find applications in different research fields, including bioinorganic

chemistry [6–9], materials science [10–12], and molecular magnetism [13–15]. In the latter case, Mn clusters hold a special place since they often possess a large number of unpaired electrons, and, in the presence of ferromagnetic exchange interactions, they can act as high spin molecules and/or magnetic refrigerants [16–18]. In addition, the combination of high spin ground state values (S) with significant uniaxial magnetic anisotropy (D), which in the case of Mn compounds is usually the result of Jahn–Teller (JT) axial elongation of Mn^{III} ions in octahedral environments, can lead to single-molecule magnetism (SMM) behaviour [19–21]. SMMs are discrete species that can exhibit the properties of bulk magnets, but at the molecular level. Thus, SMMs display slow magnetic relaxation below a characteristic blocking temperature (T_B) due to a significant energy barrier (U_{eff}) to reversal of the magnetization vector [22]. However, reorientation of magnetization cannot occur only by overcoming the U_{eff} barrier, but also through the barrier via quantum tunnelling of the magnetization (QTM) [23]. As a result of the coexistence of classical and quantum natures in such individual molecules, SMMs have been proposed for a variety of potential applications including high-density memory storage devices [24,25], quantum computing [23,26–28], and spintronics [29–32].

The synthesis of several Mn SMMs, including the first one $[Mn_{12}O_{12}(OAc)_{16}(H_2O)_4]$ [33,34], triggered interest in this area, and led to several new clusters and many synthetic strategies. As a result, Mn clusters with enhanced magnetic properties and impressive crystal structures have been reported, including the giant $[Mn_{84}]$ [35,36] and $[Mn_{70}]$ [36,37] torus-like complexes, which are the highest nuclearity 3d SMMs, and the $[Mn_{49}]$ aggregate [38], possessing a highly symmetric cuboctahedral core. These results demonstrate the special role of manganese in nanoscience and molecular magnetism, and to some extent explain why synthetic efforts are still focusing on the isolation of new Mn clusters. For these reasons, our group has had a continuing interest in the synthesis of polynuclear Mn complexes with novel structural characteristics, including large size, high nuclearities, highly symmetric metal cores, and interesting magnetic properties. To that end, we have employed several organic chelating/bridging ligands with different functionalities like (poly)alcohols [39–42] or oximates as primary organic ligands or combinations of them, following a mixed ligand approach [43–45]. Recently, these efforts were extended towards the combined use of another well-known chelate with a fruitful coordination chemistry, $(py)_2CO$, with various aliphatic diols. This ligand has afforded numerous metal clusters, mainly because of the ability of its carbonyl group to undergo metal-assisted hydrolysis or alcoholysis (ROH; R = Me, Et), forming the anionic $(py)_2CO_2^{2-}$ (gem-diol form) and $(py)_2C(OR)O^-$ (hemiketal form) groups displaying unique bridging capabilities, as illustrated by a series of studies, several of which were reported by S. P. Perlepes and coworkers [46–49]. Thus, studies from our group have shown that the combination of $(py)_2CO$ with aliphatic diols has led to the isolation of a new family of $[Mn_4M_2]$ (M = Mn or Dy, Gd, Tb) complexes, possessing an uncommon cross-shaped core [50], and the highly symmetric $[Mn_{24}]$ and $[Mn_{23}]$ supertetrahedral T4 aggregates [51].

Herein, we report five new compounds obtained from reactions involving the combination of $(py)_2CO$ with selected diols in Mn cluster chemistry. In particular, the combination of $(py)_2CO$ and 1,3-propanediol (pdH_2) or 2-methly-1,3-propanediol ($mpdH_2$) afforded complexes $[Mn_{11}O_2(OH)_2\{(py)_2CO_2\}_5((m)pd)(MeCO_2)_3(N_3)_3(NO_3)_2(DMF)_4](NO_3)$ (**1** and **2**) and $[Mn_{12}O_4(OH)_2\{(py)_2CO_2\}_4(mpd)_2(Me_3CCO_2)_4(NO_3)_4(H_2O)_6](NO_3)_2\cdot 2MeCN$ (**3**·2MeCN), whereas the use of $(py)_2CO$ in conjunction with the aromatic diol 2-(hydroxyme thyl)phenol (2-hpH_2) led to $[Mn_4(OMe)_2\{(py)_2C(OMe)O\}_2(2\text{-}hp)_2(NO_3)_2(DMF)_2]$ (**4**) and $[Mn_7\{(py)_2CO_2\}_4(2\text{-}hp)_4(NO_3)_2(DMF)_2](ClO_4)\cdot DMF$ (**5**·DMF). Interestingly, complexes **1**, **2**, **3**, and **5** possess uncommon metal cores which, to our knowledge, are reported for the first time in Mn cluster chemistry. The magnetic properties of compounds **3**–**5** were investigated through direct current (dc) magnetic susceptibility measurements, revealing the presence of dominant antiferromagnetic exchange interactions in complexes **3** and **4**, and ferromagnetic ones in **5**.

2. Materials and Methods

2.1. Materials, Physical and Spectroscopic Measurements

All manipulations were performed under aerobic conditions using materials (reagent grade) and solvents as received. Caution: Although no such behaviour was observed during the present work, perchlorate, nitrate, and azide salts are potentially explosive; they should be synthesized and used in small quantities and treated with care. Elemental analysis (C, H, and N) was performed by the in-house facilities of the University of Cyprus, Chemistry Department. IR spectra were recorded on ATR in the 4000–400 cm^{-1} range using a Shimadzu Prestige—21 spectrometer. Variable-temperature dc and ac magnetic susceptibility data were collected at the University of Florida using a Quantum Design MPMS-XL SQUID magnetometer equipped with a 7 T magnet and operating in the 1.8–400 K range. Samples were embedded in solid eicosane to prevent torquing. The ac magnetic susceptibility measurements were performed in an oscillating ac field of 3.5 G and a zero dc field. The oscillation frequencies were in the 5–1488 Hz range. Pascal's constants [52] were used to estimate the diamagnetic corrections, which were subtracted from the experimental susceptibilities to give the molar paramagnetic susceptibility (χ_M). The program PHI [53] was used to fit the magnetic data.

2.2. Syntheses

$[Mn_{11}O_2(OH)_2\{(py)_2CO_2\}_5(pd)(MeCO_2)_3(N_3)_3(NO_3)_2(DMF)_4](NO_3)\cdot 2DMF\cdot H_2O$ (**1**·2DMF·H_2O). Solid $Mn(NO_3)_2\cdot 4H_2O$ (0.75 g, 2.99 mmol) was added to a stirred solution of pdH_2 (0.30 mL, 0.32 g, 4.15 mmol) and NEt_3 (0.28 mL, 0.20 g, 2.01 mmol) in DMF (20 mL). To this solution was then added solid $(py)_2CO$ (0.10 g, 0.54 mmol), $MeCO_2Na$ (0.08 g, 0.98 mmol), and NaN_3 (0.07 g, 1.08 mmol) under continuous stirring. The resulting brown solution was stirred for 1 h, filtered, and the filtrate layered with Et_2O (1:3 *v/v*). Slow mixing gave after 1 week dark red/brown crystals of **1**, which were kept in mother liquor for X-ray analysis, or collected by filtration and dried under vacuum for other solid-state studies. Yield: ~5%. Anal. Calc. (found) for $C_{82}H_{101}N_{28}O_{38}Mn_{11}$ (**1**·2DMF·H_2O): C, 36.60 (36.36), H, 3.78 (3.92), N, 14.57 (14.39)%. Selected IR data (KBr, cm^{-1}): 3352 (sb), 2982 (m), 2932 (m), 2886 (m), 2750 (w), 2706 (w), 2482 (w), 2425 (w), 2359 (w), 2342 (w), 2118 (w), 2070 (m), 1763 (w), 1663 (m), 1584 (s), 1477 (m), 1377 (s), 1240 (m), 1157 (w), 1074 (m), 1047 (m), 1015 (m), 928 (w), 814 (m), 758 (m), 694 (m), 644 (m), 629 (s), 575 (m), 513 (m), 411 (w).

$[Mn_{11}O_2(OH)_2\{(py)_2CO_2\}_5(mpd)(MeCO_2)_3(N_3)_3(NO_3)_2(DMF)_4](NO_3)$ (**2**). This compound was prepared in the same manner as complex **1**, but by using $mpdH_2$ (0.30 mL, 0.30 g, 3.38 mmol) in place of pdH_2. After 1 week, dark red/brown crystals of **2** had appeared, which were kept in mother liquor for X-ray analysis, or collected by filtration and dried under vacuum for other solid-state studies. Yield: ~5%. Anal. Calc. (found) for $C_{77}H_{87}N_{26}O_{35}Mn_{11}$ (**2**): C, 36.40 (36.27), H, 3.45 (3.24), N, 14.33 (14.08)%. Selected IR data (KBr, cm^{-1}): 3553 (s), 3414 (sb), 3136 (s), 2828 (m), 2779 (m), 2029 (w), 1780 (m), 1710 (s), 1639 (s), 1618 (s), 1402 (s), 1242 (w), 1117 (w), 1082 (w), 1057 (w), 835 (w), 766 (m), 613 (m), 530 (m), 478 (m).

$[Mn_{12}O_4(OH)_2\{(py)_2CO_2\}_4(mpd)_2(Me_3CCO_2)_4(NO_3)_4(H_2O)_6](NO_3)_2\cdot 2MeCN$ (**3**·2MeCN). Solid $Mn(NO_3)_2\cdot 4H_2O$ (0.75 g, 2.99 mmol) was added to a stirred solution of $mpdH_2$ (0.30 mL, 0.30 g, 3.38 mmol) and NEt_3 (0.28 mL, 0.20 g, 2.01 mmol) in MeCN (20 mL). To this solution was then added solid $(py)_2CO$ (0.10 g, 0.54 mmol), and Me_3CCO_2Na (0.12 g, 0.97 mmol) under continuous stirring. The resulting brown solution was stirred for 1 h, filtered, and the filtrate left undisturbed at room temperature. After 2 weeks, dark brown crystals of **3** appeared, which were kept in mother liquor for X-ray analysis, or collected by filtration and dried under vacuum for other solid-state studies. Yield: ~59%. Anal. Calc. (found) for $C_{76}H_{104}N_{16}O_{50}Mn_{12}$ (**3**·2MeCN): C, 33.80 (33.65), H, 3.88 (3.67), N, 8.30 (8.06)%. Selected IR data (KBr, cm^{-1}): 3383 (mb), 2959 (m), 2874 (w), 2371 (w), 1765 (w), 1599 (m), 1560 (m), 1477 (m), 1437 (m), 1360 (s), 1298 (m), 1223 (m), 1155 (w), 1119 (m), 1078 (m), 1032 (s), 891 (w), 814 (w), 783 (m), 756 (w), 694 (m), 681 (m), 635 (m), 559 (m), 511 (w), 459 (w), 415 (w).

[$Mn_4(OMe)_2\{(py)_2C(OMe)O\}_2(2\text{-}hp)_2(NO_3)_2(DMF)_2$] (**4**). Solid $Mn(NO_3)_2{\cdot}4H_2O$ (0.75 g, 2.99 mmol) was added to a stirred solution of 2-hpH_2 (0.20 g, 1.61 mmol), $(py)_2CO$ (0.10 g, 0.54 mmol) and NEt_3 (0.28 mL, 0.20 g, 2.01 mmol) in a mixture of MeOH/DMF (1/1; 20 mL). The resulting brown solution was stirred for 30 min, filtered, and the filtrate layered with Et_2O (1:3 *v/v*). Slow mixing gave, after 1 week, dark brown crystals of **4**, which were kept in mother liquor for X-ray analysis, or collected by filtration and dried under vacuum for other solid-state studies. Yield: ~47%. Anal. Calc. (found) for $C_{46}H_{54}N_8O_{18}Mn_4$ (**4**): C, 45.04 (45.19), H, 4.44 (4.21), N, 9.13 (8.98)%. Selected IR data (KBr, cm^{-1}): 3419 (sb), 3139 (sb), 2960 (m), 2926 (m), 2819 (m), 2426 (w), 1734 (w), 1661 (s), 1601 (m), 1569 (w), 1474 (s), 1448 (s), 1435 (s), 1385 (s), 1313 (w), 1274 (m), 1260 (w), 1232 (w), 1222 (w), 1154 (w), 1113 (w), 1048 (m), 1026 (m), 990 (w), 935 (w), 881 (w), 783 (w), 762 (w), 725 (w), 682 (w), 635 (w), 620 (m), 575 (m), 542 (w), 517 (w), 469 (w) 455 (w), 449 (w).

[$Mn_7\{(py)_2CO_2\}_4(2\text{-}hp)_4(NO_3)_2(DMF)_2](ClO_4){\cdot}3DMF{\cdot}H_2O$ (**5**·DMF). This compound was prepared in the same manner as complex **4**, but by adding extra $NaClO_4$ (0.14 g, 1.0 mmol). After 1 week, dark brown crystals of **5** appeared, which were kept in mother liquor for X-ray analysis, or collected by filtration and dried under vacuum for other solid-state studies. Yield: ~33%. Anal. Calc. (found) for $C_{81}H_{77}N_{13}O_{29}ClMn_7$ (**5**·DMF): C, 45.97 (45.74), H, 3.67 (3.42), N, 8.60 (8.35)%. Selected IR data (KBr, cm^{-1}): 3414 (sb), 3150 (sb), 2828 (w), 2779 (w), 2033 (w), 1775 (w), 1709 (s), 1638 (s), 1616 (s), 1402 (s), 1256 (w), 1225 (w), 1159 (w), 1120 (w), 1082 (w), 1055 (w), 1001 (w), 957 (w), 877 (w), 854 (w), 821 (w), 766 (w), 729 (w), 689 (w), 629 (m), 532 (w), 476 (w), 420 (w).

2.3. Single-Crystal X-ray Crystallography

Data were collected on a Rigaku—Oxford Diffraction SuperNova A single crystal X-ray diffractometer equipped with a CCD area detector and a graphite monochromator utilizing Cu Kα radiation (λ = 1.54184 Å) or Mo Kα radiation (λ = 0.71073 Å). Selected crystals were attached to glass fiber with paratone-N oil and transferred to a goniostat for data collection. Empirical absorption corrections (multiscan based on symmetry-related measurements) were applied using CrysAlis RED software [54]. The structures were solved by direct methods using SIR92 [55], and refined on F^2 using full-matrix least-squares using SHELXL97 [56], SHELXL-2014/7 [57], and SHELXT [58]. Software packages used: CrysAlisCCD [54] for data collection, CrysAlisRED [54] for cell refinement and data reduction, WINGX for geometric calculations [59], while MERCURY [60] and Diamond [61] were used for molecular graphics. The crystal structures of compounds **1**, **2**, **3**, and **5** contain a small area of highly disordered solvent molecules. For this reason, the SQUEEZE [62] function of PLATON was employed to remove the electron density associated with these solvent molecules from the intensity data. The solvent-free model and intensity data were used for the results reported here. In order to limit the disorder of the terminal ligands or lattice solvent molecules, various restraints (SIMU, RIGU, DELU, DFIX, DANG, ISOR) have been applied in the refinement of the crystal structures. For all compounds, the non-H atoms were treated anisotropically, whereas the H atoms were placed in calculated, ideal positions and refined as riding on their respective C atoms. Unit cell parameters and structure solution and refinement data for complexes **1**–**5** are listed in Table S1.

3. Results and Discussion

3.1. Synthetic Comments

For the last several years, our group has been investigating reactions involving the combination of two different organic chelating/bridging ligands. Our first attempts focused on the combination of phenolic oximes with various diols in Mn coordination chemistry and produced high nuclearity complexes with aesthetically pleasing structures. These included a [Mn_{32}] double-decker wheel [43], which is the largest Mn/oxime SMM, a 1-D coordination polymer containing an [Mn_{40}] octagonal superstructure [44], and a [$Mn_{18}Na_6$] wheel [45], consisting of repeating [Mn_3] triangular units linked through Na^+ cations.

Recently, this synthetic methodology was extended towards the combination of $(py)_2CO$ with various aliphatic diols in Mn and Mn/4f cluster chemistry, which has led to the isolation of a new series of heterometallic $[Mn_4Ln_2]$ (Ln = Dy, Gd, Tb) complexes and their homometallic $[Mn_6]$ analogues, all based on an uncommon cross-shaped core [50]. Notably, in the homometallic and heterometallic compounds, derived from the use of phenolic oximes/diols or $(py)_2CO$/diols blend, respectively, the diols are not participating in the final structures even though they are initially used in the reaction mixture. However, reactions in the absence of the diol ligands did not produce the same results, demonstrating that although the mechanism of cluster formation is difficult to predict or explain, the presence of diols is essential for the formation of the above structures. Attempts to combine both $(py)_2CO$ and other aliphatic diols in the same structure were also successful and produced $[Mn_{24}]$ and $[Mn_{23}]$ supertetrahedral T4 clusters, incorporating both the gem-diol form of di-2-pyridyl ketone ($(py)_2CO_2^{2-}$) and 1,3-propanediol, and featuring SMM properties [51].

In the present work, we report five new Mn complexes that extend the body of results obtained from the concomitant use of $(py)_2CO$ with various diols, in this case $(m)pdH_2$ or $2\text{-}hpH_2$, and emphasize the ability of this synthetic strategy to yield new Mn clusters exhibiting unprecedented metal core topologies.

In particular, compound **1** was isolated from the investigation of reactions of the $(py)_2CO/pdH_2$ "blend" under basic conditions in the presence of azide (N_3^-) ions. Thus, the reaction of $Mn(NO_3)_2{\cdot}4H_2O$, $(py)_2CO$, and pdH_2 in the presence of NEt_3, $MeCO_2Na$, and NaN_3 in a molar ratio of ~1:0.2:1.4:0.7:0.3:0.4 in DMF resulted a brown solution which was layered with Et_2O to afford, after 1 week, dark red/brown crystals of **1** in ~5% yield. The same reaction was repeated, but using $mpdH_2$ in place of pdH_2, which yielded red/brown crystals of the isostructural complex **2** in similar yield (~5%). The formation of compounds **1** and **2** is summarized in the general Equation (1):

$$\begin{gathered}11\ Mn(NO_3)_2 + 5\ (py)_2CO + (m)pdH_2 + 3\ MeCO_2Na + 3\ NaN_3 + 1.25\ O_2 + 6.5 \\ H_2O + 4\ DMF \xrightarrow{DMF} \\ \left[Mn_{11}O_2(OH)_2\{(py)_2CO_2\}_5((m)pd)(MeCO_2)_3(N_3)_3(NO_3)_2(DMF)_4\right](NO_3) + 6 \\ NaNO_3 + 13\ HNO_3\end{gathered} \tag{1}$$

Various modifications were performed to the above-described reaction, aiming to investigate the role of the ligands employed in the synthetic route affording **1** and **2**. One of these modifications which involved the removal of N_3^- ligand from the reaction mixture, since **1** and **2** contained only three of them in their structure, two of which are terminally bound to Mn ions, afforded a new dodecanuclear Mn complex. Thus, the reaction of $Mn(NO_3)_2{\cdot}4H_2O$ with $(py)_2CO$ and $mpdH_2$, in the presence of NEt_3 and Me_3CCO_2Na in a ~1:0.2:1.1:0.7:0.3 molar ratio in MeCN, afforded dark brown crystals of compound **3**, in ~59% yield. Equation (2) summarizes the formation of **3**:

$$\begin{gathered}12\ Mn(NO_3)_2 + 4\ (py)_2CO + 2\ mpdH_2 + 4\ Me_3CCO_2Na + 2\ O_2 + 12\ H_2O \\ \xrightarrow{MeCN} \left[Mn_{12}O_4(OH)_2\{(py)_2CO_2\}_4(mpd)_2(Me_3CCO_2)_4(NO_3)_4(H_2O)_6\right] \\ (NO_3)_2 + 4\ NaNO_3 + 14\ HNO_3\end{gathered} \tag{2}$$

The extension of these studies to the use of aromatic polyols in the ligand "blend" together with $(py)_2CO$ was investigated using the diol—type ligand $2\text{-}hpH_2$. Thus, the reaction of $Mn(NO_3)_2{\cdot}4H_2O$, $(py)_2CO$, $2\text{-}hpH_2$, and NEt_3 in a molar ratio of ~1:0.2:0.5:0.7 in a mixture of MeOH/DMF (1/1) solvents resulted a brown solution which was layered with Et_2O to afford, after 1 week, dark brown crystals of **4** in ~47% yield. The formation of compound **4** is summarized in Equation (3):

$$\begin{gathered}4\ Mn(NO_3)_2 + 2\ (py)_2CO + 2\ 2-hpH_2 + 0.5\ O_2 + 4\ MeOH + 2\ DMF \xrightarrow{MeOH/DMF} \\ \left[Mn_4(OMe)_2\{(py)_2C(OMe)O\}_2(2-hp)_2(NO_3)_2(DMF)_2\right] + H_2O + 6\ HNO_3\end{gathered} \tag{3}$$

The same reaction that led to the isolation of **4** was repeated in the presence of $NaClO_4$ (0.3 equivalents), and complex **5** was produced as dark brown crystals, from slow evaporation of the solutions, in ~33% yield. The formation of compound **5** is summarized in Equation (4):

$$7\,Mn(NO_3)_2 + 4\,(py)_2CO + 4\,2-hpH_2 + NaClO_4 + 1.25\,O_2 + 1.5\,H_2O + 2\,DMF \xrightarrow{MeOH/DMF} \left[Mn_7\{(py)_2CO_2\}_4(2-hp)_4(NO_3)_2(DMF)_2\right](ClO_4) + NaNO_3 + 11\,HNO_3 \quad (4)$$

The chemical and structural identities of all the reported compounds were confirmed by single-crystal X-ray crystallography, elemental analyses (C, H, N), and IR spectroscopy.

3.2. Description of Structures

For complexes **1**–**5**, the Mn oxidation states and the protonation level of O atoms were determined by charge-balance considerations, inspection of the metric parameters, BVS calculations [63,64] (Table S2), and the observation of Jahn–Teller distortions for the octahedral Mn^{III} ions, which take the form of axial elongation.

Since compounds **1** and **2** exhibit very similar structures, with their main difference being the presence in **2** of the ligand mpd^{2-} (instead of pd^{2-}), only the structure of **1** will be described in detail. Representations of the molecular structure and the structural core of **1** and **2** are shown in Figure 1 and Figure S1, respectively. The coordination modes of the ligands are illustrated in Schemes S1 and S2. Complex **1** crystallizes in the orthorhombic space group *Pbca*. Its molecular structure consists of a $[Mn_{11}O_2(OH)_2\{(py)_2CO_2\}_5(pd)(MeCO_2)_3(N_3)_3(NO_3)_2(DMF)_4]^+$ cation, one NO_3^- counterion, as well as two DMF and one water solvent molecules. The cation of **1** features the unusual, asymmetric, mixed-valence $[Mn^{III}_5Mn^{II}_6(\mu_4\text{-}O)(\mu_3\text{-}O)(\mu_3\text{-}OH)(\mu\text{-}OH)(\mu_3\text{-}OR)_2(\mu\text{-}OR)_{10}(\mu\text{-}N_3)]^{8+}$ core in which the 11 Mn ions are held together by one of each of the following ligands, $\mu_4\text{-}O^{2-}$, $\mu_3\text{-}O^{2-}$, $\mu_3\text{-}OH^-$, $\mu\text{-}OH^-$, and one bridging end-on N_3^- group. Further bridging is provided by the doubly deprotonated alkoxido arms of one $\eta^2{:}\eta^2{:}\mu_3$ pd^{2-} ligand and five $(py)_2CO_2^{2-}$ groups. Four of the latter bridge four metal ions, either in a $\eta^1{:}\eta^2{:}\eta^2{:}\eta^1{:}\mu_4$ mode (three $(py)_2CO_2^{2-}$ anions) or in a $\eta^1{:}\eta^3{:}\eta^1{:}\eta^1{:}\mu_4$ (one of them), and the remaining one five Mn ions in a $\eta^1{:}\eta^3{:}\eta^2{:}\eta^1{:}\mu_5$ coordination mode. Additional ligation is provided by three bridging carboxylates, connecting either two or three Mn ions and adopting the *syn,syn*-$\eta^1{:}\eta^1{:}\mu$, *syn,anti*-$\eta^1{:}\eta^1{:}\mu$ and $\eta^2{:}\eta^1{:}\mu_3$ coordination modes, two chelating nitrates, two terminal azides, and four terminal DMF molecules. All Mn ions are six-coordinate with distorted octahedral geometries, except for Mn1, which is seven-coordinate in a distorted pentagonal bipyramidal geometry, and Mn3, which is five-coordinate, possessing a distorted square pyramidal geometry (τ = 0.20).

A close examination of the structure of **1** revealed the presence of strong intramolecular hydrogen-bonding interactions involving the H_2O and DMF solvent molecules and the bridging OH^- ligands (Figure S2). However, there is no evidence for direct hydrogen-bonding interactions between neighbouring cations of **1**, which are fairly well separated, as shown from the shortest Mn···Mn separation between neighbouring $[Mn_{11}]$ units, which is 8.919 Å (Mn1···Mn5).

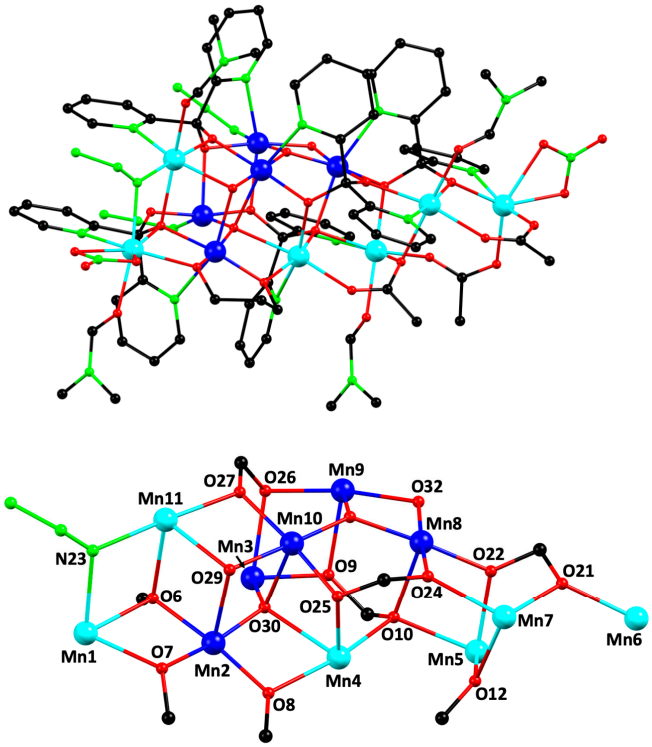

Figure 1. Ball and stick representations of (**top**) the complete structure and (**bottom**) the partially-labelled core of **1**. H atoms are omitted for clarity. Colour code: Mn^{II}, cyan; Mn^{III}, blue; N, green; O, red; C, black.

Complex **3** crystallizes in the monoclinic space group *C2/c* and its molecular structure contains a cationic cluster based on a $[Mn^{III}_8Mn^{II}_4(\mu_4\text{-}O)_2(\mu_3\text{-}O)_2(\mu_3\text{-}OH)_2(\mu\text{-}OR)_{12}]^{10+}$ core (Figure 2). The unit cell of **3** also contains two MeCN solvent molecules, and two nitrate ions that counter-balance the change of the cationic cluster. The latter could be conveniently dissected into three parts: a central $[Mn^{III}_4Mn^{II}_2O_4(OH)_2(OR)_4]^{2+}$ unit and two $[Mn^{III}_2Mn^{II}]$ trinuclear subunits located above and below the hexanuclear one. The central $[Mn^{III}_4Mn^{II}_2]$ unit consists of four edge-sharing triangles in a rod-like conformation, with all Mn ions being at the same plane. The two similar $[Mn^{III}_2Mn^{II}(OR)_4]^{4+}$ subunits comprise an Mn^{II} and two Mn^{III} ions bridged by four alkoxido O atoms in a "V-shaped" arrangement. The three parts of the core are linked together by O16 and O18 atoms corresponding to μ_4- and μ_3-O^{2-} bridges. The 12 μ-OR bridges of the structural core of the cation of **3** are provided by four $\eta^1{:}\eta^2{:}\eta^2{:}\eta^1{:}\mu_4$ $(py)_2CO_2{}^{2-}$ and two $\eta^2{:}\eta^2{:}\mu_3$ mpd^{2-} ligands (Scheme S3), while peripheral ligation is provided by four *syn,syn*-$\eta^1{:}\eta^1{:}\mu$ $Me_3CCO_2{}^-$ groups, four chelating nitrate anions, and six terminal H_2O molecules. All Mn ions are six-coordinate with distorted octahedral geometries, except for Mn3, which is seven-coordinate in a distorted pentagonal bipyramidal geometry. A close inspection of the structure of **3** revealed that the neighbouring $[Mn_{12}]$ cations are well separated, as shown from the fairly long closest intermolecular Mn···Mn separation of 7.374 Å.

Complex **4** crystallizes in the triclinic space group $P\bar{1}$ and its asymmetric unit consists of one half of the $[Mn_4(OMe)_2((py)_2C(OMe)O)_2(2\text{-}hp)_2(NO_3)_2(DMF)_2]$ molecule (Figure 3).

It possesses a defective dicubane metallic skeleton, consisting of two edge-sharing $Mn^{III}_2Mn^{II}$ triangular units. The four Mn ions are bridged by the alkoxido O atoms of two μ_3-OMe^- anions (O9), two $\eta^1{:}\eta^2{:}\eta^1{:}\mu$ $(py)_2C(OMe)O^-$ (O2), and two $\eta^1{:}\eta^2{:}\mu$ 2-hp^{2-} (O4) ligands (Scheme S4), yielding an overall $[Mn^{III}_2Mn^{II}_2(\mu_3\text{-}OMe)_2(\mu\text{-}OR)_4]^{4+}$ core. The coordination sphere of the Mn ions, which are all six-coordinate in distorted octahedral geometry, is completed by two terminal $NO_3{}^-$ ions and two DMF solvent molecules. A close inspection of the crystal packing of **4** reveals the presence of non-covalent short contacts between neighbouring $[Mn_4]$ compounds. More specifically, the coordinated

DMF molecules are involved in intermolecular CH_3-π interactions with the pyridyl rings of the $(py)_2C(OMe)O^-$ ligands, while T-shaped π-π stacking is observed between the pyridyl rings of $(py)_2C(OMe)O^-$ ligand and the phenolic rings of 2-hp^{2-}. The distance between the pyridyl C4 and the centroid of phenolic ring was found to be 3.555(9) Å (C4. . .C7C8C9C10C11C12) (Figure S3). The shortest Mn···Mn separation between adjacent neighbouring tetranuclear clusters of **4** is 9.544 Å.

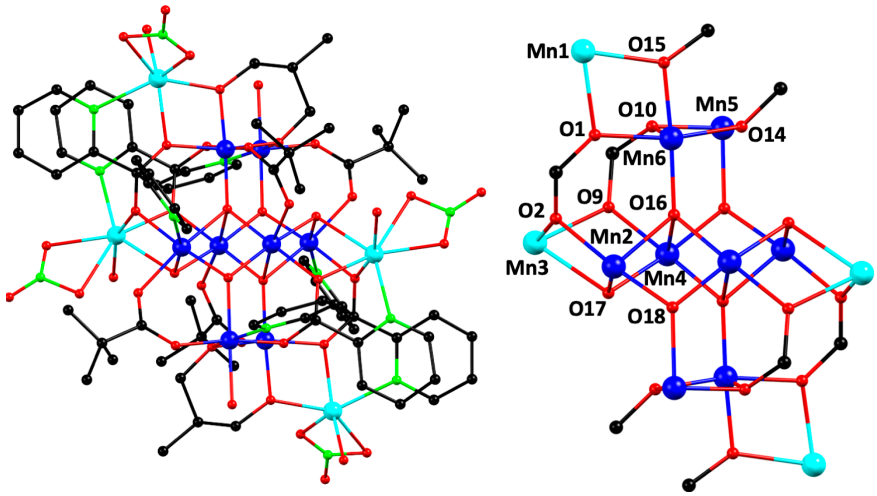

Figure 2. Ball and stick representations of (**left**) the complete structure and (**right**) the partially-labelled core of **3**. H atoms are omitted for clarity. Colour code: Mn^{II}, cyan; Mn^{III}, blue; N, green; O, red; C, black.

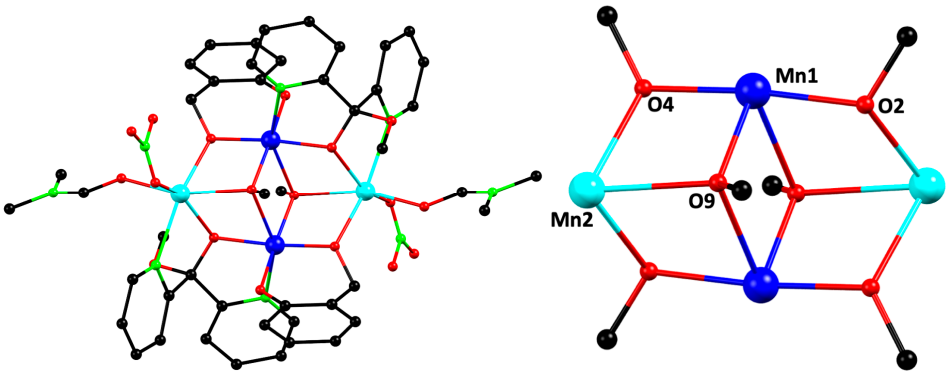

Figure 3. Ball and stick representations of (**left**) the complete structure and (**right**) the partially-labelled core of **4**. H atoms are omitted for clarity. Colour code: Mn^{II}, cyan; Mn^{III}, blue; N, green; O, red; C, black.

Complex **5** crystallizes in the monoclinic space group $P2_1/c$ and its asymmetric unit contains a $[Mn_7\{(py)_2CO_2\}_4(2\text{-}hp)_4(NO_3)_2(DMF)_2]^+$ cationic cluster, one perchlorate counterion, and one DMF solvent molecule. The structure of the cation of **5** consists of 6 vertex-sharing $[Mn_2(\mu\text{-}OR)_2]$ rhombic units that form an unusual non-planar $[Mn^{III}_5Mn^{II}_2(\mu\text{-}OR)_{12}]^{7+}$ core with a serpentine-like topology (Figure 4). The metal ions are bridged by 12 alkoxido O atoms, provided by four $\eta^1{:}\eta^2{:}\eta^2{:}\eta^1{:}\mu_4$ $(py)_2CO_2^{2-}$ groups and four $\eta^1{:}\eta^2{:}\mu$ 2-hp^{2-} ligands (Scheme S5). The peripheral ligation is completed by two terminal NO_3^- ions and two DMF solvent molecules. All Mn ions are six-coordinate in distorted octahedral coordination environment, except for Mn1 and Mn7, which are five-coordinate, possessing a distorted square pyramidal geometry (τ = 0.18 and 0.25 for Mn1 and Mn7, respectively).

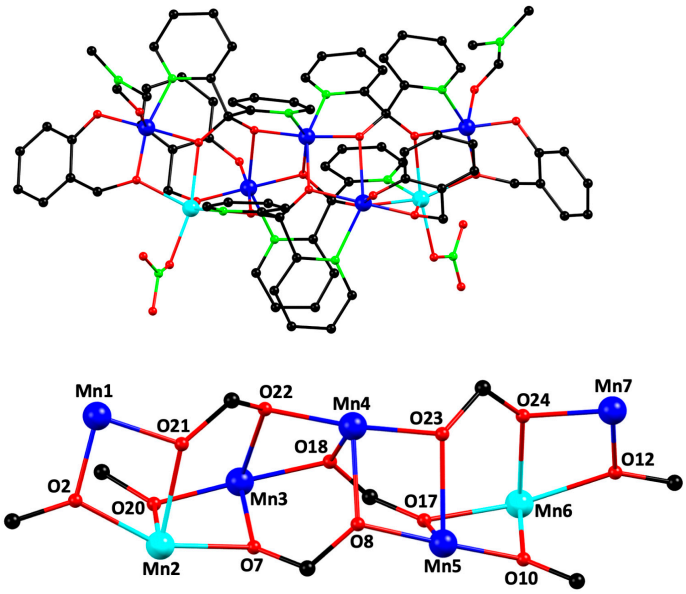

Figure 4. Ball and stick representations of (**top**) the complete structure and (**bottom**) the partially-labelled core of **5**. H atoms are omitted for clarity. Colour code: Mn^{II}, cyan; Mn^{III}, blue; N, green; O, red; C, black.

Close inspection of the crystal structure of **5** reveals that there are intermolecular π-π stacking interactions involving the pyridyl rings of $(py)_2CO_2^{2-}$ and the phenolic rings of 2-hp^{2-}, with distances ranging between 3.745 (9) and 3.868 (9) Å (Figure S4). The shortest Mn···Mn separation between adjacent neighbouring $[Mn_7]$ clusters of **5** is 8.344 Å.

The reported compounds display several novel structural features, with some of them exhibiting unprecedented asymmetric Mn/O cores. In particular, complexes **1** and **2** possess a $[Mn^{III}_5Mn^{II}_6(\mu_4\text{-O})(\mu_3\text{-O})(\mu_3\text{-OH})(\mu\text{-OH})(\mu_3\text{-OR})_2(\mu\text{-OR})_{10}(\mu\text{-N}_3)]^{8+}$ core that appears for the first time in Mn carboxylate chemistry, display a rare nuclearity [65], and a unique oxidation state level of Mn ions for undecanuclear complexes. Similarly, complex **3** is based on a multilayer $[Mn^{III}_8Mn^{II}_4(\mu_4\text{-O})_2(\mu_3\text{-O})_2(\mu_3\text{-OH})_2(\mu\text{-OR})_{12}]^{10+}$ core consisting of a central rod-like unit in which two "V-shaped" subunits are attached, while complex **5** possesses an unusual non-planar $[Mn^{III}_5Mn^{II}_2(\mu\text{-OR})_{12}]^{7+}$ core with a serpentine-like arrangement. In addition, compound **4**, despite the fact that it comprises a core that has been previously seen in coordination chemistry of 3d metal ions, [66–72] is the second example of an Mn defective dicubane structure containing a derivative of $(py)_2CO$ as ligand, the other one being the complex $[Mn_4((py)_2CO(OH))_2((py)_2CO(OCH_3))_2(N_3)_4]$ [73].

3.3. Solid-State Magnetic Susceptibility Studies

Solid-state, variable-temperature direct current (dc) magnetic susceptibility measurements were performed on powdered polycrystalline samples of **3**–**5** in a 0.1 T field and in the 5.0–300 K range; the low synthesis yields of **1** and **2** did not allow us to perform magnetic measurements on these compounds. The $\chi_M T$ versus T plots for all complexes are depicted in Figure 5.

For complex **3**, the $\chi_M T$ steadily decreases from 29.70 $cm^3mol^{-1}K$ at 300 K to 24.70 $cm^3mol^{-1}K$ at 50 K, and then it rapidly drops to a minimum of 9.75 $cm^3mol^{-1}K$ at 5.0 K. The $\chi_M T$ at 300 K is smaller than the spin-only (g = 2) value of 41.50 $cm^3mol^{-1}K$ for four Mn^{II} and eight Mn^{III} non-interacting ions, indicating the presence of dominant antiferromagnetic exchange interactions. The $\chi_M T$ at 5.0 K suggests a non-zero spin ground state value of S_T = 3 or 4.

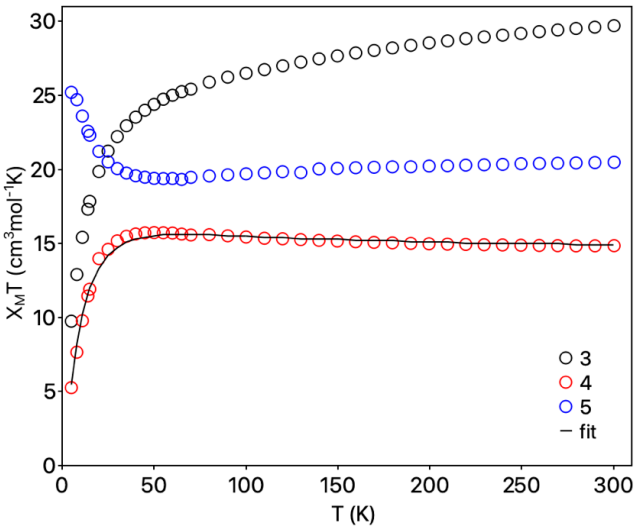

Figure 5. Temperature dependence of $\chi_M T$ for complexes **3**, **4**, and **5** in a field of 0.1 T. The solid black line represents the fit of the experimental data obtained for complex **4**.

In the case of **4**, the $\chi_M T$ at 300 K is 14.85 cm^{3}mol^{-1}K, remains almost stable up to 50 K, and then decreases rapidly to a minimum of 5.26 cm^{3}mol^{-1}K at 5.0 K. The $\chi_M T$ value at 300 K is in agreement with the spin-only (g = 2) value of 14.75 cm^{3}mol^{-1}K for 2 Mn^{II} and 2 Mn^{III} non-interacting ions. The shape of the curve indicates the existence of dominant antiferromagnetic exchange interactions and a small spin ground state (possibly S_T = 1). In order to quantify the strength of the intramolecular magnetic exchange interactions, the magnetic susceptibility data for compound **4** were fit using program PHI [53]. The system was modeled by using two exchange parameters (Figure S5), J_{wb} and J_{bb}, accounting for the peripheral Mn^{II}···Mn^{III} and the central Mn^{III}···Mn^{III} interactions, respectively. The spin Hamiltonian used is shown in Equation (5).

$$\hat{H} = -2J_{wb}\left(\vec{S}_1\vec{S}_2 + \vec{S}_2\vec{S}_3 + \vec{S}_3\vec{S}_4 + \vec{S}_4\vec{S}_1\right) - 2J_{bb}\vec{S}_1\vec{S}_3 + \mu_B g\left(\sum_{i=1}^{4}\vec{S}_i\right)H \quad (5)$$

The fit gave the following parameters: J_{wb} = −0.33(1) cm^{-1}, J_{bb} = 6.28(1) cm^{-1}, and g = 1.98(1), revealing weak antiferromagnetic interactions along the peripheral Mn^{II}···Mn^{III} ions and ferromagnetic interactions between the central Mn^{III}···Mn^{III} ions, and suggesting a spin ground state S_T = 1. The obtained coupling constants and g values are within the range reported for other Mn_4 clusters with similar structural core, in the majority of which the metal ions are ferromagnetically coupled [66–72]. However, there are cases reporting antiferromagnetic exchange interactions between the Mn ions of such tetranuclear clusters [74,75].

For complex **5**, the experimental $\chi_M T$ value at 300 K (20.48 cm^{3}mol^{-1}K) is slightly lower than the spin-only (g = 2) value for 2 Mn^{II} and 5 Mn^{III} non-interacting ions (23.75 cm^{3}mol^{-1}K). Upon cooling, the $\chi_M T$ decreases slightly to 19.38 cm^{3}mol^{-1}K at 50 K and then it increases rapidly to reach a maximum of 25.20 cm^{3}mol^{-1}K at 5.0 K. This low temperature increase of the $\chi_M T$ is indicative of the presence of dominant ferromagnetic exchange interactions in complex **5**, while the maximum $\chi_M T$ value at 5 K suggests a spin ground state of S_T = 6 or 7.

To obtain additional information about the spin ground states, S_T, and the potential presence of slow relaxation of magnetization (indicative of SMM behaviour) in complexes **3**–**5**, alternating current (ac) magnetic susceptibility studies were performed. Data were collected using a 3.5 G ac field and a 1000 Hz oscillation frequency over the temperature range 1.8–15 K. In the case of complex **3**, the in-phase signal (plotted as $\chi'_M T$ vs. T) decreases from 19.00 cm^{3}mol^{-1}K at 15.0 K to 5.87 cm^{3}mol^{-1}K at 1.8 K (Figure S6, left). The decrease

of $\chi'_M T$ with decreasing T is suggestive of the presence of low-lying excited states with S greater than the ground state, as expected for a system with dominant antiferromagnetic exchange interactions. Extrapolation of the $\chi'_M T$ data from above ∼6.0 K to 0 K gives a value of ∼6 $cm^3mol^{-1}K$, which is indicative of a spin ground state S_T∼3 for g = 2.0. These findings are consistent with the results obtained from the dc data. Additionally, no out-of-phase χ''_M signals were observed for complex **3** (Figure S6, right), indicating that this compound does not exhibit SMM behaviour.

In the case of complex **4**, the in-phase $\chi'_M T$ signal (Figure S7, left) displayed an almost linear decrease from ∼12.40 $cm^3mol^{-1}K$ at 15 K to ∼2.73 $cm^3mol^{-1}K$ at 1.8 K. Extrapolation of the $\chi'_M T$ data from above ∼6.0 K to 0 K gives a value of ∼2.0 $cm^3mol^{-1}K$, suggestive of a spin ground state S_T∼1 (for g = 2.0), in agreement with the conclusion from the dc studies. Complex **4** does not show any frequency-dependent out-of-phase (χ''_M) ac signals down to 1.8 K (Figure S7, right), possibly due to its small S_T value.

The $\chi'_M T$ vs. T plot for complex **5** (Figure S8, left) shows a steep increase with decreasing T from 23.71 $cm^3mol^{-1}K$ at 15 K to a plateau value of ∼27 $cm^3mol^{-1}K$ at ∼5 K. This behaviour indicates a spin ground state S_T∼7, in line with the conclusions from the dc studies. The drop of $\chi'_M T$ at lower T may be due to the existence of weak intermolecular interactions. Below ∼2.5 K, there is a drop in $\chi'_M T$ accompanied by an increase in the χ''_M vs. T (Figure S8, right). However, the signal is very weak, and no peak maxima were observed, indicating that **5** may display slow magnetic relaxation, but below 1.8 K, the operating limit of our SQUID magnetometer.

4. Conclusions

The syntheses, crystal structures, and magnetic properties of five new Mn clusters (**1**–**5**) are reported. They were derived from a synthetic strategy that involves the concomitant use of $(py)_2CO$ and selected diols in Mn cluster chemistry. The reported compounds display novel structural features and some of them unprecedented structural cores (**1**–**3** and **5**). Magnetism studies indicated the presence of dominant antiferromagnetic exchange interactions in compounds **3** and **4**, and ferromagnetic ones in **5**. The latter also exhibits weak out-of-phase ac signals at low T, suggesting that it might be a weak SMM. This work extends the body of results obtained from the concomitant use of $(py)_2CO$ with various diols in Mn cluster chemistry and emphasizes the ability of this synthetic strategy to yield compounds possessing novel structural features. This possibly happens because of the exceptional bridging capability of $(py)_2CO$'s derivatives and polyols, which are able to afford high nuclearity Mn clusters with aesthetically pleasing structures. Future studies will involve the use of additional diol ligands, including pyridyl diols, in conjunction with $(py)_2CO$ in Mn cluster chemistry.

Supplementary Materials: The following supporting information can be downloaded at: https://www.mdpi.com/article/10.3390/chemistry5030115/s1. Table S1. Crystal data and structural refinement parameters for compounds **1**·2DMF·H_2O, **2**, **3**·2MeCN, **4** and **5**·DMF. Table S2. Bond valence sum (BVS) calculations for Mn ions in **1**–**5**. Figure S1. Ball and stick representation of the complete structure of **2**. H atoms are omitted for clarity. Colour code: Mn^{II}, cyan; Mn^{III}, blue; N, green; O, red; C, black. Figure S2. Hydrogen bonding in **1**, including interactions of a lattice H_2O (O38) molecule with a bridging OH^- (O32) anion (O38···O32 = 2.672 (2) Å) and an O atom of a lattice DMF molecule (O36) with a bridging OH^- (O29) anion (O36···O29 = 2.756 (4) Å). Colour code: Mn^{II}, cyan; Mn^{III}, blue; N, green; O, red; C, black. H atoms are omitted for clarity. Figure S3. Intermolecular CH_3-π interactions between a coordinated DMF (C16) molecule with a pyridyl ring (C17C18C19C20C21N4) of the $(py)_2C(OMe)O^-$ ligand (C16...C17C18C19C20C21N4 = 3.677 (9) Å), and T-shaped π-π stacking between a pyridyl ring (C4) of $(py)_2C(OMe)O^-$ ligand and a phenolic ring (C7C8C9C10C11C12) of 2-hp^{2-} anion (C4...C7C8C9C10C11C12 = 3.555 (9) Å) in **4**. Colour code: Mn^{II}, cyan; Mn^{III}, blue; N, green; O, red; C, black. H atoms are omitted for clarity. Figure S4. Intermolecular π-π stacking in **5**, including interactions (left) of the pyridyl rings (C45C46C47C48C49N8) of $(py)_2CO_2^{2-}$ anions (C45C46C47C48C49N8...C45C46C47C48C49N8 = 3.745 (9) Å), and (right) of a pyridyl ring (C13) of $(py)_2CO_2^{2-}$ and a phenolic ring (C1C2C3C4C5C6) of 2-hp^{2-} anions (C13...C1C2C3C4C5C6 =

3.868 (9) Å) of two adjacent cations of **5**. Colour code: Mn^{II}, cyan; Mn^{III}, blue; N, green; O, red; C, black. H atoms are omitted for clarity. Figure S5. J-coupling scheme employed for the elucidation of magnetic exchange interactions in **4**. Figure S6. Temperature dependence of the in-phase $\chi'_M T$ product (left) and out-of-phase χ''_M (right) ac susceptibility signal of **3** in a 3.5 G field oscillating at 1000 Hz frequency. Figure S7. Temperature dependence of the in-phase $\chi'_M T$ product (left) and out-of-phase χ''_M (right) ac susceptibility signal of **4** in a 3.5 G field oscillating at 1000 Hz frequency. Figure S8. Temperature dependence of the in-phase $\chi'_M T$ product (left) and out-of-phase χ''_M (right) ac susceptibility signal of **5** in a 3.5 G field oscillating at 1000 Hz frequency. Scheme S1. Schematic representation of the coordination modes of $(py)_2CO_2^{2-}$ and pd^{2-} ligands in complex **1**. Scheme S2. Schematic representation of the coordination modes of $(py)_2CO_2^{2-}$ and pd^{2-} ligands in complex **2**. Scheme S3. Schematic representation of the coordination modes of $(py)_2CO_2^{2-}$ and mpd^{2-} ligands in complex **3**. Scheme S4. Schematic representation of the coordination modes of $(py)_2C(OMe)O^-$ and $2\text{-}hp^{2-}$ ligands in complex **4**. Scheme S5. Schematic representation of the coordination modes of $(py)_2CO_2^{2-}$ and $2\text{-}hp^{2-}$ ligands in complex **5**.

Author Contributions: Conceptualization, A.J.T.; methodology, K.S., E.E.M. and C.P.; software, K.S., A.D.F., N.P. and D.I.A.; validation, A.J.T. and G.C.; formal analysis, K.S., A.D.F., N.P. and D.I.A.; investigation, K.S. and A.D.F.; resources, A.J.T.; data curation, K.S., A.D.F., N.P. and D.I.A.; writing—original draft preparation, D.I.A.; writing—review and editing, D.I.A., G.C. and A.J.T.; visualization, D.I.A. and A.D.F.; supervision, A.J.T.; project administration, A.J.T.; funding acquisition, A.J.T. All authors have read and agreed to the published version of the manuscript.

Funding: This research was funded by the Cyprus Research and Innovation Foundation Research Grant "EXCELLENCE/0421/399", which is co-funded by the Republic of Cyprus and the European Regional Development Fund. G.C. thanks the US National Science Foundation for support (CHE-1900321) and the University of Florida.

Data Availability Statement: The crystallographic data for complexes **1**–**5** have been deposited in the Cambridge Structural Database and assigned the following numbers CCDC 2278744-2278748.

Conflicts of Interest: The authors declare no conflict of interest.

References

1. Papatriantafyllopoulou, C.; Moushi, E.E.; Christou, G.; Tasiopoulos, A.J. Filling the Gap between the Quantum and Classical Worlds of Nanoscale Magnetism: Giant Molecular Aggregates Based on Paramagnetic 3d Metal Ions. *Chem. Soc. Rev.* **2016**, *45*, 1597–1628. [CrossRef]
2. Maniaki, D.; Pilichos, E.; Perlepes, S.P. Coordination Clusters of 3d-Metals That Behave as Single-Molecule Magnets: Synthetic Routes and Strategies. *Front. Chem.* **2018**, *6*, 461. [CrossRef]
3. Dearle, A.E.; Cutler, D.J.; Coletta, M.; Lee, E.; Dey, S.; Sanz, S.; Fraser, H.W.L.; Nichol, G.S.; Rajaraman, G.; Schnack, J.; et al. An $[Fe^{III}_{30}]$ Molecular Metal Oxide. *Chem. Commun.* **2022**, *58*, 52–55. [CrossRef]
4. Deng, Y.; Wu, Y.; Li, Z.; Jagličić, Z.; Gupta, R.K.; Tung, C.; Sun, D. Synthesis, Structure, and Optical-Response Magnetic Property of a Heteroarene-azo Functionalized Mn_{19} Cluster. *Chin. J. Chem.* **2023**, *41*, 1667–1672. [CrossRef]
5. Lee, K.H.K.; Aebersold, L.; Peralta, J.E.; Abboud, K.A.; Christou, G. Synthesis, Structure, and Magnetic Properties of an Fe_{36} Dimethylarsinate Cluster: The Largest 'Ferric Wheel'. *Inorg. Chem.* **2022**, *61*, 17256–17267. [CrossRef] [PubMed]
6. Mukherjee, S.; Stull, J.A.; Yano, J.; Stamatatos, T.C.; Pringouri, K.; Stich, T.A.; Abboud, K.A.; Britt, R.D.; Yachandra, V.K.; Christou, G. Synthetic Model of the Asymmetric $[Mn_3CaO_4]$ Cubane Core of the Oxygen-Evolving Complex of Photosystem II. *Proc. Natl. Acad. Sci. USA* **2012**, *109*, 2257–2262. [CrossRef] [PubMed]
7. Zhang, C.; Chen, C.; Dong, H.; Shen, J.-R.; Dau, H.; Zhao, J. A Synthetic Mn_4Ca-Cluster Mimicking the Oxygen-Evolving Center of Photosynthesis. *Science* **2015**, *348*, 690–693. [CrossRef]
8. Signorella, S.; Hureau, C. Bioinspired Functional Mimics of the Manganese Catalases. *Coord. Chem. Rev.* **2012**, *256*, 1229–1245. [CrossRef]
9. Najafpour, M.M.; Zaharieva, I.; Zand, Z.; Maedeh Hosseini, S.; Kouzmanova, M.; Hołyńska, M.; Tranca, I.; Larkum, A.W.; Shen, J.-R.; Allakhverdiev, S.I. Water-Oxidizing Complex in Photosystem II: Its Structure and Relation to Manganese-Oxide Based Catalysts. *Coord. Chem. Rev.* **2020**, *409*, 213183. [CrossRef]
10. Thuijs, A.E.; Li, X.-G.; Wang, Y.-P.; Abboud, K.A.; Zhang, X.G.; Cheng, H.-P.; Christou, G. Molecular Analogue of the Perovskite Repeating Unit and Evidence for Direct MnIII-CeIV-MnIII Exchange Coupling Pathway. *Nat. Commun.* **2017**, *8*, 500. [CrossRef]
11. Deng, Y.-K.; Su, H.-F.; Xu, J.-H.; Wang, W.-G.; Kurmoo, M.; Lin, S.-C.; Tan, Y.-Z.; Jia, J.; Sun, D.; Zheng, L.-S. Hierarchical Assembly of a $\{Mn^{II}_{15}Mn^{III}_4\}$ Brucite Disc: Step-by-Step Formation and Ferrimagnetism. *J. Am. Chem. Soc.* **2016**, *138*, 1328–1334. [CrossRef]
12. Das Gupta, S.; Stewart, R.L.; Chen, D.-T.; Abboud, K.A.; Cheng, H.-P.; Hill, S.; Christou, G. Long-Range Ferromagnetic Exchange Interactions Mediated by Mn–Ce^{IV}–Mn Superexchange Involving Empty 4f Orbitals. *Inorg. Chem.* **2020**, *59*, 8716–8726. [CrossRef]

13. Zabala-Lekuona, A.; Seco, J.M.; Colacio, E. Single-Molecule Magnets: From Mn12-ac to Dysprosium Metallocenes, a Travel in Time. *Coord. Chem. Rev.* **2021**, *441*, 213984. [CrossRef]
14. Coronado, E. Molecular Magnetism: From Chemical Design to Spin Control in Molecules, Materials and Devices. *Nat. Rev. Mater.* **2020**, *5*, 87–104. [CrossRef]
15. Abbasi, P.; Quinn, K.; Alexandropoulos, D.I.; Damjanović, M.; Wernsdorfer, W.; Escuer, A.; Mayans, J.; Pilkington, M.; Stamatatos, T.C. Transition Metal Single-Molecule Magnets: A $\{Mn_{31}\}$ Nanosized Cluster with a Large Energy Barrier of ∼60 K and Magnetic Hysteresis at ∼5 K. *J. Am. Chem. Soc.* **2017**, *139*, 15644–15647. [CrossRef]
16. Evangelisti, M.; Brechin, E.K. Recipes for Enhanced Molecular Cooling. *Dalton Trans.* **2010**, *39*, 4672–4676. [CrossRef] [PubMed]
17. Evangelisti, M.; Luis, F.; de Jongh, L.J.; Affronte, M. Magnetothermal Properties of Molecule-Based Materials. *J. Mater. Chem.* **2006**, *16*, 2534–2549. [CrossRef]
18. Oyarzabal, I.; Zabala-Lekuona, A.; Mota, A.J.; Palacios, M.A.; Rodríguez-Diéguez, A.; Lorusso, G.; Evangelisti, M.; Rodríguez-Esteban, C.; Brechin, E.K.; Seco, J.M.; et al. Magneto-thermal Properties and Slow Magnetic Relaxation in Mn(ii)Ln(iii) Complexes: Influence of Magnetic Coupling on the Magneto-caloric Effect. *Dalton Trans.* **2022**, *51*, 12954–12967. [CrossRef] [PubMed]
19. Aromí, G.; Brechin, E.K. Synthesis of 3d Metallic Single-Molecule Magnets. In *Single-Molecule Magnets and Related Phenomena*; Winpenny, R., Ed.; Springer: Berlin/Heidelberg, Germany, 2006; pp. 1–67.
20. Milios, C.J.; Winpenny, R.E.P. Cluster-Based Single-Molecule Magnets. In *Molecular Nanomagnets and Related Phenomena*; Gao, S., Ed.; Springer: Berlin/Heidelberg, Germany, 2015; pp. 1–109.
21. Pedersen, K.S.; Bendix, J.; Clérac, R. Single-molecule Magnet Engineering: Building-block Approaches. *Chem. Commun.* **2014**, *50*, 4396–4415. [CrossRef]
22. Bagai, R.; Christou, G. The Drosophila of Single-Molecule Magnetism: $[Mn_{12}O_{12}(O_2CR)_{16}(H_2O)_4]$. *Chem. Soc. Rev.* **2009**, *38*, 1011–1026. [CrossRef]
23. Gatteschi, D.; Sessoli, R. Quantum Tunneling of Magnetization and Related Phenomena in Molecular Materials. *Angew. Chem. Int. Ed.* **2003**, *42*, 268–297. [CrossRef]
24. Bogani, L.; Wernsdorfer, W. Molecular Spintronics Using Single-Molecule Magnets. *Nat. Mater.* **2008**, *7*, 179. [CrossRef]
25. Urdampilleta, M.; Klyatskaya, S.; Cleuziou, J.P.; Ruben, M.; Wernsdorfer, W. Supramolecular Spin Valves. *Nat. Mater.* **2011**, *10*, 502. [CrossRef]
26. Tiron, R.; Wernsdorfer, W.; Aliaga-Alcalde, N.; Christou, G. Quantum Tunneling in a Three-Dimensional Network of Exchange-Coupled Single-Molecule Magnets. *Phys. Rev. B* **2003**, *68*, 140407. [CrossRef]
27. Hill, S.; Edwards, R.S.; Aliaga-Alcalde, N.; Christou, G. Quantum Coherence in an Exchange-Coupled Dimer of Single-Molecule Magnets. *Science* **2003**, *302*, 1015–1018. [CrossRef]
28. Vincent, R.; Klyatskaya, S.; Ruben, M.; Wernsdorfer, W.; Balestro, F. Electronic Read-out of a Single Nuclear Spin Using a Molecular Spin Transistor. *Nature* **2012**, *488*, 357. [CrossRef]
29. Aguilà, D.; Barrios, L.A.; Velasco, V.; Roubeau, O.; Repollés, A.; Alonso, P.J.; Sesé, J.; Teat, S.J.; Luis, F.; Aromí, G. Heterodimetallic [LnLn′] Lanthanide Complexes: Toward a Chemical Design of Two-Qubit Molecular Spin Quantum Gates. *J. Am. Chem. Soc.* **2014**, *136*, 14215–14222. [CrossRef]
30. Moreno-Pineda, E.; Godfrin, C.; Balestro, F.; Wernsdorfer, W.; Ruben, M. Molecular Spin Qudits for Quantum Algorithms. *Chem. Soc. Rev.* **2018**, *47*, 501–513. [CrossRef]
31. Moreno-Pineda, E.; Wernsdorfer, W. Measuring Molecular Magnets for Quantum Technologies. *Nat. Rev. Phys.* **2021**, *3*, 645–659. [CrossRef]
32. Aravena, D.; Ruiz, E. Spin Dynamics in Single-Molecule Magnets and Molecular Qubits. *Dalton Trans.* **2020**, *49*, 9916–9928. [CrossRef]
33. Sessoli, R.; Gatteschi, D.; Caneschi, A.; Novak, M.A. Magnetic Bistability in a Metal-ion Cluster. *Nature* **1993**, *365*, 141. [CrossRef]
34. Christou, G.; Gatteschi, D.; Hendrickson, D.N.; Sessoli, R. Single-Molecule Magnets. *MRS Bull.* **2000**, *25*, 66–71. [CrossRef]
35. Tasiopoulos, A.J.; Vinslava, A.; Wernsdorfer, W.; Abboud, K.A.; Christou, G. Giant Single-Molecule Magnets: A $\{Mn_{84}\}$ Torus and Its Supramolecular Nanotubes. *Angew. Chem. Int. Ed.* **2004**, *43*, 2117–2121. [CrossRef]
36. Hale, A.R.; Abboud, K.A.; Christou, G. Synthetic Factors Determining the Curvature and Nuclearity of the Giant Mn_{70} and Mn_{84} Clusters with a Torus Structure of ∼4 nm Diameter. *Inorg. Chem.* **2023**, *62*, 6020–6031. [CrossRef]
37. Vinslava, A.; Tasiopoulos, A.J.; Wernsdorfer, W.; Abboud, K.A.; Christou, G. Molecules at the Quantum-Classical Nanoparticle Interface: Giant Mn_{70} Single-Molecule Magnets of ∼4 nm Diameter. *Inorg. Chem.* **2016**, *55*, 3419–3430. [CrossRef]
38. Manoli, M.; Alexandrou, S.; Pham, L.; Lorusso, G.; Wernsdorfer, W.; Evangelisti, M.; Christou, G.; Tasiopoulos, A.J. Magnetic 'Molecular Oligomers' Based on Decametallic Supertetrahedra: A Giant Mn_{49} Cuboctahedron and Its $Mn_{25}Na_4$ Fragment. *Angew. Chem. Int. Ed.* **2016**, *55*, 679–684. [CrossRef]
39. Moushi, E.E.; Masello, A.; Wernsdorfer, W.; Nastopoulos, V.; Christou, G.; Tasiopoulos, A.J. A Mn_{15} single-molecule magnet consisting of a supertetrahedron incorporated in a loop. *Dalton Trans.* **2010**, *39*, 4978–4985. [CrossRef]
40. Charalambous, M.; Zartilas, S.M.; Moushi, E.E.; Papatriantafyllopoulou, C.; Manos, M.J.; Stamatatos, T.C.; Mukherjee, S.; Nastopoulos, V.; Christou, G.; Tasiopoulos, A.J. Discrete and encapsulated molecular grids: Homometallic Mn_{15} and heterometallic $Mn_{24}Ni_2$ aggregates. *Chem. Commun.* **2014**, *50*, 9090–9093. [CrossRef]
41. Charalambous, M.; Moushi, E.E.; Nguyen, T.N.; Mowson, A.M.; Christou, G.; Tasiopoulos, A.J. $[Mn_{14}]$ "Structural Analogues" of Well-Known $[Mn_{12}]$ Single-Molecule Magnets. *Eur. J. Inorg. Chem.* **2018**, *2018*, 3905–3912. [CrossRef]

42. Skordi, K.; Papatriantafyllopoulou, C.; Zartilas, S.; Poole, K.M.; Nastopoulos, V.; Christou, G.; Tasiopoulos, A.J. Homometallic $\{Mn_{10}\}$ and heterometallic $\{Mn_6Ca_4\}$ supertetrahedra exhibiting an unprecedented $\{Mn^{III}{}_9Mn^{II}\}$ oxidation state level and heterometal ions distribution. *Polyhedron* **2018**, *151*, 433–440. [CrossRef]
43. Manoli, M.; Inglis, R.; Manos, M.J.; Nastopoulos, V.; Wernsdorfer, W.; Brechin, E.K.; Tasiopoulos, A.J. A $[Mn_{32}]$ Double-Decker Wheel. *Angew. Chem. Int. Ed.* **2011**, *50*, 4441–4444. [CrossRef]
44. Manoli, M.; Inglis, R.; Manos, M.J.; Papaefstathiou, G.S.; Brechin, E.K.; Tasiopoulos, A.J. A 1-D coordination polymer based on a Mn_{40} octagonal super-structure. *Chem. Commun.* **2013**, *49*, 1061–1063. [CrossRef]
45. Manoli, M.; Inglis, R.; Piligkos, S.; Yanhua, L.; Wernsdorfer, W.; Brechin, E.K.; Tasiopoulos, A.J. A hexameric $[Mn^{III}{}_{18}Na_6]$ wheel based on $[Mn^{III}{}_3O]^{7+}$ sub-units. *Chem. Commun.* **2016**, *52*, 12829–12832. [CrossRef]
46. Stamatatos, T.C.; Efthymiou, C.G.; Stoumpos, C.C.; Perlepes, S.P. Adventures in the Coordination Chemistry of Di-2-pyridyl Ketone and Related Ligands: From High-Spin Molecules and Single-Molecule Magnets to Coordination Polymers, and from Structural Aesthetics to an Exciting New Reactivity Chemistry of Coordinated Ligands. *Eur. J. Inorg. Chem.* **2009**, *2009*, 3361–3391.
47. Mayans, J.; Font-Bardia, M.; Escuer, A. Lithium cations in a self-assembled electrostatic nanocapsule. *Dalton Trans.* **2019**, *48*, 16158–16161. [CrossRef] [PubMed]
48. Papaefstathiou, G.S.; Perlepes, S.P. Families of Polynuclear Manganese, Cobalt, Nickel and Copper Complexes Stabilized by Various Forms of Di-2-pyridyl Ketone. *Comments Inorg. Chem.* **2002**, *23*, 249–274. [CrossRef]
49. Tasiopoulos, A.J.; Perlepes, S.P. Diol-type ligands as central 'players' in the chemistry of high-spin molecules and single-molecule magnets. *Dalton Trans.* **2008**, *41*, 5537–5555. [CrossRef]
50. Savva, M.; Skordi, K.; Fournet, A.D.; Thuijs, A.E.; Christou, G.; Perlepes, S.P.; Papatriantafyllopoulou, C.; Tasiopoulos, A.J. Heterometallic $Mn^{III}{}_4Ln_2$ (Ln = Dy, Gd, Tb) Cross-Shaped Clusters and Their Homometallic MnIII4MnII2 Analogues. *Inorg. Chem.* **2017**, *56*, 5657–5668. [CrossRef]
51. Skordi, K.; Anastassiades, A.; Fournet, A.D.; Kumar, R.; Schulze, M.; Wernsdorfer, W.; Christou, G.; Nastopoulos, V.; Perlepes, S.P.; Papatriantafyllopoulou, C.; et al. High nuclearity structurally—Related Mn supertetrahedral T4 aggregates. *Chem. Commun.* **2021**, *57*, 12484–12487. [CrossRef]
52. Bain, G.A.; Berry, J.F. Diamagnetic Corrections and Pascal's Constants. *J. Chem. Educ.* **2008**, *85*, 532. [CrossRef]
53. Chilton, N.F.; Anderson, R.P.; Turner, L.D.; Soncini, A.; Murray, K.S. PHI: A powerful new program for the analysis of anisotropic monomeric and exchange-coupled polynuclear d- and f-block complexes. *J. Comput. Chem.* **2013**, *34*, 1164–1175. [CrossRef] [PubMed]
54. Loeffen, P. ; *Oxford Diffraction. CrysAlis CCD and CrysAlis RED*; Oxford Diffraction Ltd.: Abingdon, UK, 2008.
55. Altomare, A.; Cascarano, G.; Giacovazzo, C.; Guagliardi, A.; Burla, M.C.; Polidori, G.; Camalli, M. SIR92—A program for automatic solution of crystal structures by direct methods. *J. Appl. Crystallogr.* **1994**, *27*, 435. [CrossRef]
56. Shelxl, S.G.M. *Program for the Refinement of Crystal Structures*; University of Göttingen: Göttingen, Germany, 1997.
57. Sheldrick, G.M. *SHELXL-2014, Program for the Refinement of Crystal Structures*; University of Göttingen: Göttingen, Germany, 2014.
58. Oxford Diffraction. *CrysAlis CCD and CrysAlis RED, Version 1.71*; Oxford Diffraction: Oxford, UK, 2007.
59. Farrugia, L.J. WinGX suite for small-molecule single-crystal crystallography. *J. Appl. Crystallogr.* **1999**, *32*, 837–838. [CrossRef]
60. Macrae, C.F.; Edgington, P.R.; McCabe, P.; Pidcock, E.; Shields, G.P.; Taylor, R.; Towler, M.; Streek, J.V.D. Mercury: Visualization and analysis of crystal structures. *J. Appl. Crystallogr.* **2006**, *39*, 453–457. [CrossRef]
61. Brandenburg, K.; Putz, H. *Diamond*; Crystal Impact GbR: Bonn, Germany, 2006.
62. van der Sluis, P.; Spek, A.L. BYPASS: An effective method for the refinement of crystal structures containing disordered solvent regions. *Acta Crystallogr. Sect. A* **1990**, *46*, 194–201. [CrossRef]
63. Liu, W.; Thorp, H.H. Bond valence sum analysis of metal-ligand bond lengths in metalloenzymes and model complexes. 2. Refined distances and other enzymes. *Inorg. Chem.* **1993**, *32*, 4102–4105. [CrossRef]
64. Brown, I.D.; Altermatt, D. Bond-valence parameters obtained from a systematic analysis of the Inorganic Crystal Structure Database. *Acta Crystallogr. Sect. B* **1985**, *41*, 244–247. [CrossRef]
65. Koumousi, E.S.; Lazari, G.; Grammatikopoulos, S.; Papatriantafyllopoulou, C.; Manos, M.J.; Perlepes, S.P.; Tasiopoulos, A.J.; Christou, G.; Stamatatos, T.C. Rare nuclearities in Mn/oxo cluster chemistry: Synthesis and characterization of a mixed-valence $\{Mn^{II/III}{}_{11}\}$ complex bearing acetate and salicylhydroximate(-3) bridging/chelating ligands. *Polyhedron* **2021**, *206*, 115298. [CrossRef]
66. Yoo, J.; Yamaguchi, A.; Nakano, M.; Krzystek, J.; Streib, W.E.; Brunel, L.-C.; Ishimoto, H.; Christou, G.; Hendrickson, D.N. Mixed-Valence Tetranuclear Manganese Single-Molecule Magnets. *Inorg. Chem.* **2001**, *40*, 4604–4616. [CrossRef]
67. Yang, E.-C.; Harden, N.; Wernsdorfer, W.; Zakharov, L.; Brechin, E.K.; Rheingold, A.L.; Christou, G.; Hendrickson, D.N. Mn_4 single-molecule magnets with a planar diamond core and S=9. *Polyhedron* **2003**, *22*, 1857–1863. [CrossRef]
68. Wittick, L.M.; Jones, L.F.; Jensen, P.; Moubaraki, B.; Spiccia, L.; Berry, K.J.; Murray, K.S. New mixed-valence $Mn^{II}{}_2Mn^{III}{}_2$ clusters exhibiting an unprecedented MnII/III oxidation state distribution in their magnetically coupled cores. *Dalton Trans.* **2006**, *12*, 1534–1543. [CrossRef] [PubMed]
69. Ako, A.M.; Mereacre, V.; Hewitt, I.J.; Clérac, R.; Lecren, L.; Anson, C.E.; Powell, A.K. Enhancing single molecule magnet parameters. Synthesis, crystal structures and magnetic properties of mixed-valent Mn_4 SMMs. *J. Mater. Chem.* **2006**, *16*, 2579–2586. [CrossRef]

70. Karotsis, G.; Teat, S.J.; Wernsdorfer, W.; Piligkos, S.; Dalgarno, S.J.; Brechin, E.K. Calix[4]arene-Based Single-Molecule Magnets. *Angew. Chem. Int. Ed.* **2009**, *48*, 8285–8288. [CrossRef] [PubMed]
71. Saha, A.; Abboud, K.A.; Christou, G. New Mixed-Valent Mn Clusters from the Use of N,N,N′,N′-Tetrakis(2-hydroxyethyl)ethylene diamine (edteH$_4$): Mn$_3$, Mn$_4$, Mn$_6$, and Mn$_{10}$. *Inorg. Chem.* **2011**, *50*, 12774–12784. [CrossRef] [PubMed]
72. Nguyen, T.N.; Abboud, K.A.; Christou, G. A Mn$_4$ single-molecule magnet with the defective-dicubane structure from the use of pyrenecarboxylic acid. *Polyhedron* **2013**, *66*, 171–178. [CrossRef]
73. Papaefstathiou, G.S.; Escuer, A.; Raptopoulou, C.P.; Terzis, A.; Perlepes, S.P.; Vicente, R. Defective Double-Cubane, Tetranuclear Manganese(II) and Cobalt(II) Complexes with Simultaneous μ1,1-Azido and μ-O Bridges. *Eur. J. Inorg. Chem.* **2001**, *2001*, 1567–1574. [CrossRef]
74. Stamatatos, T.C.; Adam, R.; Raptopoulou, C.P.; Psycharis, V.; Ballesteros, R.; Abarca, B.; Perlepes, S.P.; Boudalis, A.K. The first member of a second generation family of ligands derived from metal-ion assisted reactivity of di-2,6-(2-pyridylcarbonyl)pyridine: Synthesis and characterization of a MnII/III4 rhombus. *Inorg. Chem. Commun.* **2012**, *15*, 73–77. [CrossRef]
75. Vignesh, K.R.; Langley, S.K.; Gartshore, C.J.; Moubaraki, B.; Murray, K.S.; Rajaraman, G. What Controls the Magnetic Exchange and Anisotropy in a Family of Tetranuclear {Mn$_2^{II}$Mn$_2^{III}$} Single-Molecule Magnets? *Inorg. Chem.* **2017**, *56*, 1932–1949. [CrossRef]